S. Tamimi*, A. Andrade-Campos and J. Pinho-da-Cruz

Modelling the Portevin-Le Chatelier effects in aluminium alloys: a review

DOI 10.1515/jmbm-2015-0008

Abstract: Plastic deformation processes are among the most demanding processes in manufacturing because they lead to different microstructure features in the materials produced. Various dislocation patterns can be induced by plastic strain under different conditions. A serrated yielding/jerky flow in some dilute alloys, such as aluminium-magnesium alloys during plastic deformation, is a well-known phenomenon under certain regimes of strain rate and temperature, as reported in a significant number of works. The serrated features in these materials reflect the so-called Portevin-Le Chatelier effects. These undesirable effects are due to the interaction between solute atoms and mobile dislocation during the plastic deformation, which is known as dynamic strain ageing. There are a significant number of theoretical and numerical investigations that have focused on describing the serrated behaviours of these materials during plastic deformation. Hence, the fundamental objective of this paper is to provide a general review of different constitutive modelling in regards this feature. The typical material models and new constitutive models describing this feature are presented. In addition, applications of the models are provided along with their respective advantages and disadvantages.

Keywords: aluminium-magnesium alloys; constitutive modelling; dynamic strain ageing; Portevin-Le Chatelier effects.

1 Introduction

Dynamic strain aging (DSA) is a well-known phenomenon occurring in many alloys as a result of the interaction between solute atoms and mobile dislocations during plastic deformation (e.g. [1, 2]). As opposed to DSA, in static strain aging (SSA) (e.g. [3, 4]), the solute-dislocation interactions occur only after plastic deformation. DSA and SSA phenomena are known to bring loss in ductility in the metallic materials. In addition, in some cases, these may result in the heterogeneous plastic deformation and the localisation of the plastic deformation in to slip-bands. As a consequence of interactions between solute atoms and dislocations, there exist two kinds of propagative patterns during plastic deformation: the Lüders bands and the Portevin-Le Chatelier (PLC) bands, which are caused by SSA and DSA, respectively. Both features are undesirable and should be avoided in manufacturing processes.

Piobert and Lüders first reported the Lüders phenomenon in low carbon steels [5, 6]. They have shown that a Lüders band travels along the specimen during the tensile test at a constant cross-head speed. The observed angle of front line is approximately 50° from the sample axis, which is the most common slip direction of <111> in BCC materials. Figure 1 schematically illustrates the formation of Lüders bands. As can be seen, after a drop in stress from the upper yield point to the lower yield point due to the elastic relaxation of the rest of the sample, the plastic front of the Lüders bands moves at a constant lower yield stress level.

The nucleation and movement of the Lüders band in these materials at room temperature are associated with the collective unpinning of the dislocations that are initially locked at the upper yield point. The time required for alloying atoms to diffuse into the core dislocations and lock them is longer than the total time of the load applying; hence, no further repinning can occur. The stress required to push the dislocations is lower than the upper yield point. Consequently, the lower yield stress corresponds to the propagation of the Lüders band (Figure 1). However, SSA (via increasing the temperature for a sufficient time) can lead to the diffusion of the alloying atoms into the dislocations' core, which causes the appearance of Lüders bands in the next plastic deformation.

Meanwhile, the serration feature of PLC was first reported by Savart [8]. However, the details of this observation were documented by Le Chatelier [9] for steel between 80°C and 250°C, and by Portevin and Le Chatelier

***Corresponding author: S. Tamimi,** Center for Mechanical Technology and Automation, TEMA, Departmento de Engenharia Mecânica, Universidade de Aveiro, Portugal,
e-mail: saeed.tamimi@ua.pt; saeed.tamimi@gmail.com
A. Andrade-Campos and J. Pinho-da-Cruz: Center for Mechanical Technology and Automation, TEMA, Departmento de Engenharia Mecânica, Universidade de Aveiro, Portugal

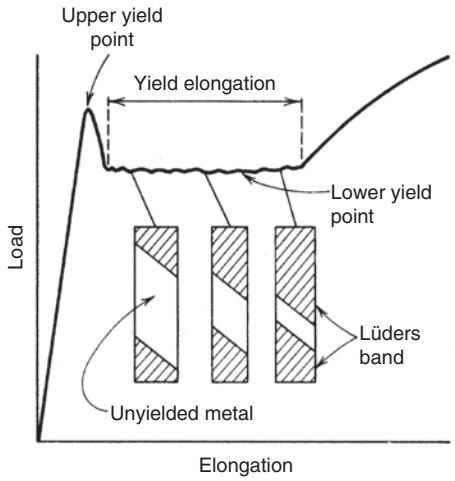

Figure 1: A schematic illustration of the propagation of Lüders bands in a stress-strain curve [7].

[10] for aluminium (Al) alloys at room temperature. Therefore, the serration phenomenon was named Portevin-Le Chatelier effect (PLC effect). Once the sample containing the alloying elements is taken under a plastic load, a discontinuous behaviour occurs consisting of stress drops and reloading sequences. It should be noted that each load drop is related to the nucleation of a localised deformation band that occurs within a range of strain rates and temperatures. Later, many studies on the PLC effect, as one type of defect in various metallic materials, have been carried out (e.g. [11–13]). In a microscopic point of view, dislocation distorts the surrounding lattice, thus causing an elastic stress field that acts on the neighbouring solute atoms. During plastic deformation, when mobile dislocations are being blocked by dislocations tangles, a cloud of solute is formed around it in order to reduce the distortion in the crystal. This occurs with solute segregations by preferred pipe diffusion and the mobile dislocation is effectively pinned (Figure 2). With the aid of effective stress, obstacles can be overcome by thermally activated dislocation motion; this unpinning process of dislocation, combined with the long range dislocation interactions, causes a stress drop on macroscopic stress curve [14].

The conditions of the occurrence of the PLC effect in terms of strain, strain rate and temperature have been taken into consideration by a considerable number of authors [e.g. 3]. The PLC phenomena occur in a specific range of temperature and strain rate in Al alloys [15, 16]. Figure 3 illustrates a typical range of strain rate-temperature for a jerky flow of the PLC phenomena in an Al-magnesium (Mg) alloy, which has been obtained using the experimental measurements and using an Arrhenius type equation [16].

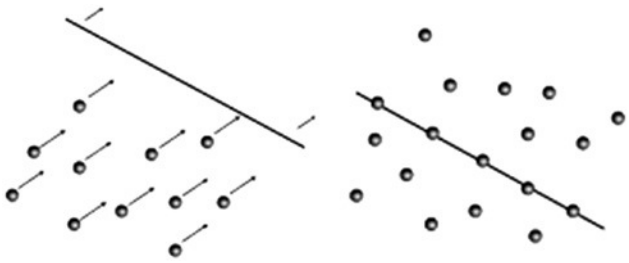

Figure 2: Diffusion of alloying atoms towards mobile dislocations (DSA).

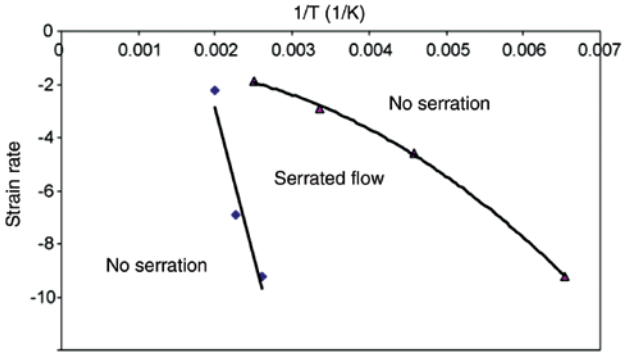

Figure 3: Range of strain rate-temperature for the occurrence of serrated follow of the PLC in the AA-5083 alloy [16].

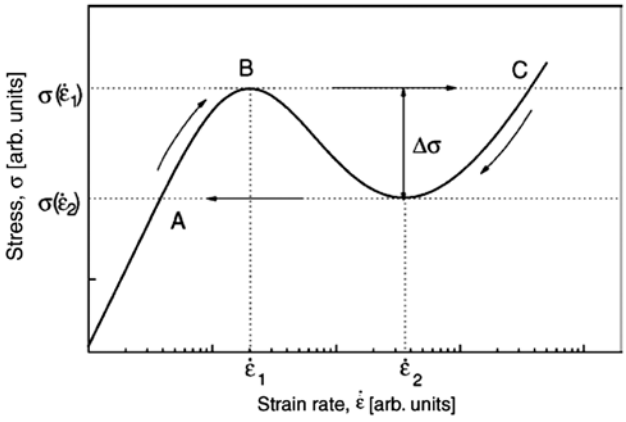

Figure 4: Flow stress dependence of the strain rate for an Al-Mg alloy at room temperature [17].

Furthermore, Figure 4 illustrates a nonlinear feature of stress vs. strain rate, namely, the existence of a range of $\dot{\varepsilon}$, where the flow stress exhibits a negative sensitivity to strain rate. This results in an N-shaped dependence of stress on $\dot{\varepsilon}$. Such behaviour is stress rate- and temperature-dependent. Here, the arrows indicate the cyclic orbit corresponding to unstable plastic flow [18, 19].

In polycrystals deformed with a constant imposed strain rate falling in the negative strain rate sensitivity

range, three types of serrated curves are commonly distinguished [20]. These correspond to different dynamics of strain localisation evolving from the so-called type C to type B and to type A when the strain rate is increased or when the temperature is reduced: type A serrations are associated with the repetitive continuous propagation of deformation bands nucleated at a certain point, often at a specimen end, and moving along the specimen; type B serrations correspond to a hopping propagation of localised bands in the axial direction of the sample; and type C serrations occur when localised deformation bands appear in a spatially non-correlated manner. As in the case of type B, each stress drop reflects the formation of a single localised band. As noted previously, the DSA phenomenon occurs for a certain range of temperature and strain rate; in some cases, a critical strain level has to be reached for serrated yielding to take place.

In general, DSA and the PLC effects have been the subject of numerous experimental and theoretical studies. In the past decades, numerical modelling using the finite element (FE) method has also been used to investigate the PLC effect. These studies aim to represent the spatio-temporal evolution of the local mechanical variables using appropriate constitutive laws. There are various types of material models that attempt to describe the DSA and the PLC effects. In the present work, a review of the material models describing the spatio-temporal aspects of the PLC phenomena is presented. In models based on the macroscopic description of deformation bands, the negative strain rate sensitivity is explicitly defined, and serrations are obtained from strain rate jumps. The other type of materials models rely on a microscopic description of the DSA based on the internal variable of ageing time. Here, the negative strain rate sensitivity and serrations are implicit consequences of constitutive equations. Additionally, some more sophisticated models have been reported in previous works based on thermodynamic features. In this work, the application of these material models and their capability to explain the serration behaviours of the materials though plastic deformation are discussed.

2 Micromechanical constitutive formulation

2.1 The fundamental approach

A simple relation between the flow stress (σ) the plastic strain (ε) and the plastic strain rate ($\dot{\varepsilon}$), first suggested by Penning [18], can be written as:

$$\sigma = h\varepsilon + F(\dot{\varepsilon}), \tag{1}$$

where h is the strain hardening coefficient that is assumed constant for simplicity, and $F(\dot{\varepsilon})$ is a function exhibiting a range of negative strain rate sensitivity. This expression results in the N-shape behaviour shown in Figure 4. Numerical modelling studies of the PLC effect have been reported in previous works. This approach, previously suggested by McCormick [21, 22], Estrin and McCormick [23] and McCormick et al. [24], was later revised by McCormick and Ling [25] to simulate the serration behaviour of the materials. The significant aspects of the PLC effect (e.g. PLC instabilities and their critical plastic strain) can be successfully predicted using this micromechanical constitutive model.

The features of the PLC effect can be simulated by discretising a tensile sample in a number of small sections. The constitutive equation in each single section is simultaneously solved while taking into account the constraint of constant crosshead velocity. Here, according to the demonstrated works [21, 22, 24, 26], the DSA influence on the following stress is taken into account by adding a term to Eq. (1). This additive term depends on the solute concentration at the blocked mobile dislocations. Hence, the applied stress σ is given as:

$$\sigma = h\varepsilon + S_i \ln\left(\frac{\dot{\varepsilon}}{\dot{\varepsilon}_0}\right) + \beta C, \tag{2}$$

where S_i is the instantaneous strain rate sensitivity of the flow stress in the absence of solute effects; the parameter β represents the strength of dislocation pinning by solutes; and C indicates the average solute concentration around dislocations. The term of βC depends on the average waiting time t_w of dislocations at localised obstacles (or dislocation tangles), which is inversely proportional to the plastic strain rate, $\dot{\varepsilon}$. The average waiting time can be written as:

$$t_w = \frac{\Omega}{\dot{\varepsilon}}, \tag{3}$$

where Ω is a strain increment produced when all arrested dislocations overcome localised obstacles and advance to the next pinned configuration. The variation of C with the waiting time can be described [27–29] by:

$$C = C_m\left[1\text{-}\exp\left(-\frac{C_0}{C_m}\left(\frac{t_w}{\tau}\right)^p\right)\right]. \tag{4}$$

In this equation, C_m is a saturation value of the solute concentration at dislocations, and C_0 is the nominal solute concentration in the crystal bulk, in the following form:

$$C_m = C_0 \exp\left(\frac{W}{k_B T}\right). \quad (5)$$

The parameter W represents the binding energy between a solute atom and a dislocation, and k_B is the Boltzmann constant. It is noticeable that the binding energy W influences the parameter β in Eq. (2), whose estimated order of magnitude is $\frac{w}{b^3}$. The parameter b is the Burgers vector of the dislocation. Here, Eq. (4) involves the characteristic time τ, which is related to solute diffusion to dislocations. This characteristic time depends on the temperature calculated as follows:

$$\tau = \tau_0 \exp\left(\frac{Q}{k_B T}\right), \quad (6)$$

where Q is the activation energy for solute migration, and the pre-exponential factor τ_0 is constant.

In Eq. (4), regarding the classical Cottrell-Bilby theory [30], the exponent p is 2/3. However, a smaller value of 1/3 has also been reported in [31]. The solute concentration given by Eq. (4) obeys the Cottrell-Bilby type power-law for small waiting times and saturates at C, for large t_w. Substituting Eqs. (3–6) in Eq. (2), $\sigma(\dot{\varepsilon})$ can be written as:

$$\sigma(\dot{\varepsilon}) = S_i \ln\left(\frac{\dot{\varepsilon}}{\dot{\varepsilon}_0}\right) + \beta C_m \left[1 - \exp\left(-\left(\frac{\dot{\varepsilon}^*}{\dot{\varepsilon}}\right)^p\right)\right], \quad (7)$$

where

$$\dot{\varepsilon}^* = \left(\frac{\Omega}{\tau_0}\right) \exp\left(-\frac{(Q + W/p)}{K_B T}\right). \quad (8)$$

The non-monotonic strain rate-dependent behaviour seen in Figure 4 can be explained by Eq. (7). In the large strain rate limit (i.e. $\dot{\varepsilon}_2 < \dot{\varepsilon}$ in Figure 4), the last term is negligible and the logarithmic dependence, which is characterised by a solute-free material, is recovered. However, for small strain rates (i.e. $\dot{\varepsilon} < \dot{\varepsilon}_1$ in Figure 4) when the waiting times are long enough for the solute atoms around dislocations reach saturation concentration, Eq. (7) can be written as:

$$\sigma = S_i \ln\left(\frac{\dot{\varepsilon}}{\dot{\varepsilon}_0}\right) + \beta C_m. \quad (9)$$

It is obvious that the low strain rate range of the flow stress vs. $\ln\left(\frac{\dot{\varepsilon}}{\dot{\varepsilon}_0}\right)$ curve is simply vertically displaced by βC_m, with respect to the high strain rate ranges. Hence, there is a transition region between the two strain rate limits and the stress decreases by strain rate (i.e. $\dot{\varepsilon}_1 < \dot{\varepsilon} < \dot{\varepsilon}_2$ in Figure 4). In other words, in this range of strain rate, the strain rate sensitivity is negative, resulting in the N-shaped curve of Figure 4. The influence of temperature on the flow stress-strain rate curve plotted in this figure can also be perused. Regarding Eq. (5), with the rising temperature, βC_m decreases between two ascending branches of the curve shown in Figure 4. Additionally, an increase of T results in a decrease of the slope of the curve, which is due to S_i being inversely proportional to temperature in these ranges of strain rates. Based on Eq. (8), the positions of $\dot{\varepsilon}_1$ and $\dot{\varepsilon}_2$ shift to higher strain rates as $\dot{\varepsilon}^*$ grows with temperature; simultaneously, their differences also increase (Figure 4). This means that the range of negative strain rate sensitivity becomes smoother in the curve of $\sigma(\dot{\varepsilon})$ vs. $\dot{\varepsilon}$. It can also occur when the nominal solute concentration C_0 is reduced.

In general, the mentioned constitutive parameters should be experimentally determined by measurements. A comparison of the results obtained by the numerical study of the PLC effect based on the transient constitutive model for DSA and experimental observation in an Al alloy indicates that the numerical simulations are in good agreement with experimental measurements [32, 33]. Moreover, Jiang et al. [34] produced the elastic shrinkage outside an avalanche-like PLC deformation band using this model with modified boundary conditions. In that work, numerical simulations were carried out for three types of PLC effects at different constant applied strain rates in a conventional tensile test, which were found to be in good agreement with the experimental observations (Figure 5). They also investigated the dynamic interactions between dislocation and diffusing solute atoms by the constitutive equations.

Furthermore, Lebyodkin et al. [35, 36] investigated the statistics of the stress drops associated with the PLC effect in an AI-Mg alloy (AA-5xxx) both experimentally and theoretically for single crystals and polycrystals. They used the constitutive models for dynamically strain ageing materials discussed above [21–24, 26] to describe the temporal behaviour associated with the PLC effect. Additionally, the localised deformation band patterns characteristic of the PLC effect was simulated using this model. A principal feature of the model used in their work is a dynamisation of the N-shaped curve proposed by Kubin, where it had been shown that the elastic loading occurring during the waiting time leads to a deformation. The authors of that work also indicated that the proposed model provides an adequate description of both the statistics of stress discontinuities as well as the spatial features of the PLC effect. The model is able to reproduce the important features of the material behaviour in the PLC regime (e.g. different

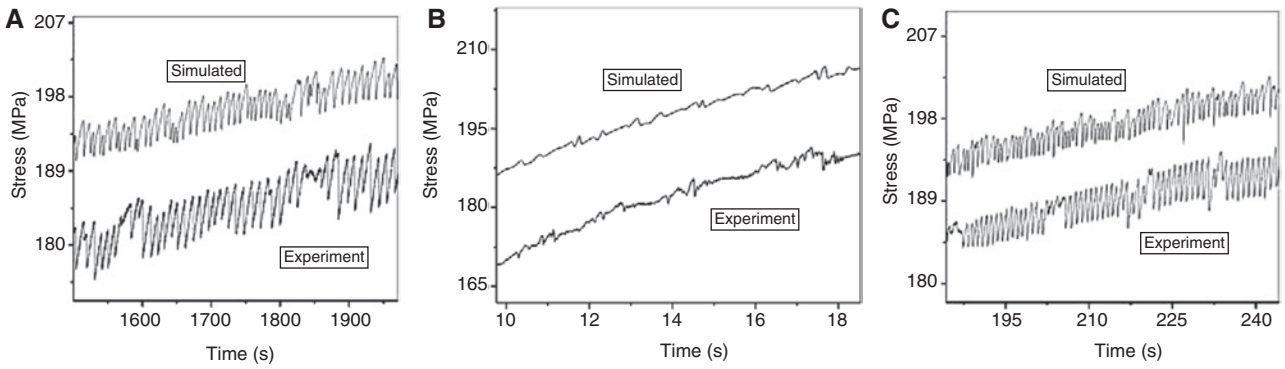

Figure 5: Experimental and simulated observation of three PLC types in tensile test at different applied strain rates. (A) Type A, 5 E-3 s^{-1}; (B) type B, 5E-4 s^{-1}; and (C) type C, 5E-5 s^{-1} [34].

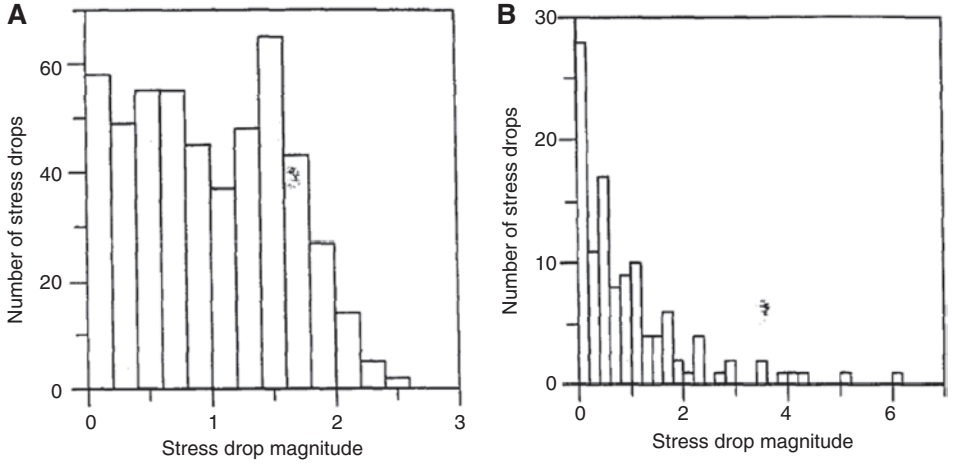

Figure 6: Simulated statistical distribution of the stress drops vs. different stress drop magnitudes. (A) 1E-4 s^{-1} strain rate and (B) 4E-4 s^{-1} strain rate [35].

types of serrations, the variation of the character of the stress drop statistics with changing deformation conditions, and spatial deformation patterns). Figure 6 indicates a statistical observation of stress drops for various stress drop magnitudes in an Al-Mg alloy for two different strain rates. These studies also indicated that a combination of a local constitutive law capturing the temporal aspects of the PLC effect with a certain type of spatial coupling can result in a simple and efficient model describing the spatio-temporal behaviour of a dynamically strained ageing material exhibiting the PLC effect.

2.2 Developed approach and its application

Zhang et al. [37] revised the model presented in the previous section. An elasto-viscoplastic constitutive law accounts for DSA through a new internal variable, the ageing time and a hardening term for three-dimensional finite element analyses. The shape of PLC bands in AA-6xxx alloys was then investigated through FE analysis using this model. In order to conduct 3D simulations of the serration features and PLC effect, the constitutive model suggested by McCormick was reformulated for multiaxial loading [38]. Here, the increment of the total strain rate tensor (i.e. $\Delta\varepsilon_{ij}^{t}$) is defined by the sum of the elastic (i.e. $\Delta\varepsilon_{ij}^{e}$) and plastic (i.e. $\Delta\varepsilon_{ij}^{p}$) strain tensor increments given by:

$$\Delta\varepsilon_{ij}^{t}=\Delta\varepsilon_{ij}^{e}+\Delta\varepsilon_{ij}^{p}. \tag{10}$$

According to Hooke's law, the elastic part of the equation can be written in terms of the stress tensor increment $\Delta\sigma_{ij}$:

$$\Delta\varepsilon_{ij}^{e}=C_{ijkl}\Delta\sigma_{kl}, \text{ where } C_{ijkl}=\frac{1+\upsilon}{E}\left(\delta_{ik}\delta_{jl}-\frac{\upsilon}{1+\upsilon}\delta_{ij}\delta_{kl}\right). \tag{11}$$

Here, υ and E are the Poisson's ratio and the Young's modulus, respectively. Meanwhile, the plastic strain increment tensor, $\Delta\varepsilon_{ij}^{p}$, can be written as:

$$\Delta\varepsilon_{ij}^{p}=\dot{\varepsilon}_{ij}^{p}\Delta t, \tag{12}$$

where Δt is the time increment. Assuming a plastically isotropic material, the plastic strain rate tensor $\dot{\varepsilon}_{ij}^{p}$ is written in terms of the stress tensor σ_{ij} or the deviatoric stress tensor of s_{ij}. The corresponding equivalent von Mises quantities can be defined as:

$$\Delta\varepsilon_{ij}^{p}=\sqrt{\frac{2}{3}\dot{\varepsilon}_{ij}^{p}\dot{\varepsilon}_{ij}^{p}}\ \text{and}\ \sigma_{v}=\sqrt{\frac{2}{3}s_{ij}s_{ij}}. \tag{13}$$

Regarding the Prandtl-Reuss equation, the plastic strain rate tensor is given by:

$$\dot{\varepsilon}_{ij}^{p}=\frac{3}{2}\frac{\dot{\varepsilon}^{p}}{\sigma_{v}}s_{ij}. \tag{14}$$

Estrin and McCormick [23], McCormick et al. [24] and Estrin [38] suggested the equivalent plastic strain rate of $\dot{\varepsilon}^{p}$ as follows:

$$\dot{\varepsilon}^{p}=\dot{\varepsilon}_{0}\exp\left(\frac{\sigma_{v}\text{-}\sigma_{d}}{S}\text{-}P_{1}C_{s}'\right). \tag{15}$$

This equation is valid only for the non-negativity of the exponent. The stress σ_{d}, representing the strain hardening effect, is related to the dislocation density evolution, which is given by:

$$\sigma_{d}=d_{1}+d_{2}\left(1\text{-}\exp\left(\text{-}\frac{\varepsilon^{p}}{d_{3}}\right)\right). \tag{16}$$

As explained, the strain rate sensitivity (i.e. S) depends on stress and subsequently strain. This parameter has been obtained by experimental measurements for an Al alloy in the work of Ling and McCormick [33] using the following equation:

$$S=s_{1}+s_{2}(\varepsilon^{p})^{\frac{1}{2}}. \tag{17}$$

In Eqs. (15–17), $\dot{\varepsilon}_{0}$, P_{1}, d_{1}, d_{2}, d_{3}, s_{1}, and s_{2} are constants (the strain rate dependence of d_{1}, d_{2} and d_{3} [38] is neglected), and ε^{p} is the (von Mises) equivalent plastic strain. The non-dimensional solute concentration corresponds to:

$$C_{s}=(1\text{-}\exp(\text{-}P_{2}(\varepsilon^{p})^{\alpha}(t_{a}^{n})))C_{m}. \tag{18}$$

The maximal overconcentration is C_{m} when the effective ageing time t_{a} tends to infinity, and P_{2} characterises the rate of saturation of solute atoms around dislocations. The parameters α and n are constants pertaining to the measurements of Ling and McCormick [33].

An important assumption regarding the work of McCormick et al. [24] concerns the ageing and waiting times. The effective ageing time (i.e. t_{a}) is not equal to the average waiting time when a dislocation is arrested at localised obstacles (i.e. t_{w}). Hence, according to McCormick's work, the effective ageing time (t_{a}) is considered to relax towards t_{w} with time t. The time derivative of t_{a} is obtained by the following relationship:

$$\frac{dt_{a}}{dt}=1\text{-}\frac{t_{a}}{t_{w}}. \tag{19}$$

Regarding the previously mentioned works, the waiting time t_{w} is related to the equivalent plastic strain rate via Eq. (3) (i.e. $t_{w}=\frac{\Omega}{\dot{\varepsilon}_{p}}$). Here, the strain dependence of Ω can be obtained using the dislocation model [21, 22, 24]. This developed model gives a realistic description of the spatio-temporal dynamic behaviours of the three types of PLC effects by including the spatial coupling.

Kok et al. [39, 40] employed a crystal plasticity model embedded in an FE framework to study the PLC effect in constant cross-head velocity-controlled tensile tests. They used a constitutive law based on the Zhang model and introduced the model into a crystal plasticity law. The constitutive model of Zhang was later modified by Graff et al. [41, 42] through the introduction of a thermally activated elasto-viscoplastic law. This formulation, for example, was used by Belotteau et al. [43] to predict both static (i.e. in Lüders bands) and dynamic strain ageing (i.e. the PLC effects) of steel over a large range of temperatures and strain rates. Maziere et al. [44] used the same constitutive model to simulate round smooth and notched specimens of a Ni based superalloy. Hopperstad et al. [45] used an anisotropic elasto-viscoplastic model including the McCormick model for DSA. In the works of Graff and Belotteau, the PLC effects in notched and cracked specimens were numerically investigated with 2D models. Accordingly, Wenman and Chard-Tuckey [46] applied a 3D model of a notched specimen to study the strain localisation stemming from static ageing including residual stress and plastic strain obtained by preloading in compression.

Benallal et al. [47] used a phenomenological elasto-viscoplastic model based on the work of Penning [18] to investigate the serration features in tensile tests with smooth axisymmetric samples (with and without U-notch) at various strain rates. The simulated results of Benallal's work are in good agreement with the experimental observations reported in a previous work [48]. In order to

simulate the negative strain rate sensitivity being able to predict strain localisation bands (i.e. PLC bands), different strain hardening laws have been used in this model for different strain rates.

Manach et al. [49] used McCormick's model to study the PLC effects in an Al-Mg alloy. They used shear tests at room temperature in order to compare the predicted load drops and kinetics of the bands with the experimental data. They also considered anisotropy and kinematic hardening by using an anisotropic yield criterion and a nonlinear kinematic hardening given by:

$$f(\sigma, \bar{\varepsilon}^P, t_a)=\sigma_v\text{-}R\text{-}P_1C_s(\bar{\varepsilon}^P, t_a), \tag{20}$$

where σ_v is the von Mises equivalent stress and R is the isotropic work hardening defined as:

$$R=\sigma_y+Q(1\text{-}\exp(\text{-}b\bar{\varepsilon}^P)). \tag{21}$$

The term $P_1C_s(\bar{\varepsilon}^P, t_a)$ in Eq. (20) is the extra-hardening induced by strain ageing suggested by Zhang et al. [37]. Regarding Eq. (18), C_s is a function of both internal variables of the model, the equivalent plastic strain and the ageing time t_a. The plastic strain follows a flow rule derived from a viscoplastic potential Ω given by:

$$\Omega(f)=K\dot{\varepsilon}_0\cosh\left(\frac{f^+}{K}\right). \tag{22}$$

In this equation, $\dot{\varepsilon}_0$ represents the strain rate sensitivity coefficient, and K *is* a weighting coefficient of the viscous part of the stress, with f^+ being the positive part of the yield criterion. The equivalent plastic strain rate tensor is defined by the plastic conservation principle in the form of:

$$\dot{\bar{\varepsilon}}^P=\frac{\partial\Omega}{\partial\sigma}=\Omega'(f)\frac{\partial f}{\partial\sigma}. \tag{23}$$

Additionally the ageing time increment, Δt_a, can be calculated using the increment of the plastic strain, w. This can be produced when all locked dislocations escape from their obstacles. The ageing time increment, Δt_a, can be obtained using the following equation:

$$\Delta t_a=1\text{-}\frac{t_a}{w}\dot{\bar{\varepsilon}}^P, \tag{24}$$

where the increment of the plastic strain, w, leads the incremental strain resulting from the jump of unpinned dislocations, and has a significant influence on the transition process between pinned and unpinned states. According to Wang et al. [50], decreasing this value may promote strain localisation.

Regarding Eq. (24), the ageing time depends on $\dot{\bar{\varepsilon}}^P$, which has a maximum point, i.e. it increases until it reaches the maximum value of the waiting time $\frac{w}{\dot{\bar{\varepsilon}}^P}$ and then decreases to zero. The PLC effects and strain localisation features appear after this point. The hardening caused by DSA depends on the C_s, which increases with ageing time from C_s=0 (the unpinned situation) to C_s=1 (the fully pinned situation) or inversely when a PLC band crosses. An extra stress P_1 [shown in Eq. (20)] is required to switch between both situations while the kinetics of the pinning process can be controlled by the parameter n in Eq. (18). Manach et al. [49] showed that the McCormick model is capable of predicting the PLC features. The amplitude is similar to those that have been measured experimentally. Additionally, their study indicated the different types of PLC (i.e. A and B PLC bands) as a function of the strain rate with respect to the stress drop distribution. Strain, time and strain rate jumps are also in good agreement with experimental observations (Figure 7).

Furthermore, it has been shown that the kinematics of the bands using the McCormick model is in agreement with experimental observations. In the shear stress direction and its perpendicular directions, the speed of growth of the PLC bands is faster. This leads to the production of different bands instead of a well-defined band as observed in the experimental results. Additionally, Manach et al. [49] used the following model of Johnson-Cook [51, 52] to study the PLC effect in Al-Mg alloy due to its simplicity:

$$\bar{\sigma}=[A+B\bar{\varepsilon}^{P^n}]\left[1+D\ln\left(\frac{\dot{\bar{\varepsilon}}_p}{\dot{\varepsilon}_0}\right)\right][1\text{-}T^m]. \tag{25}$$

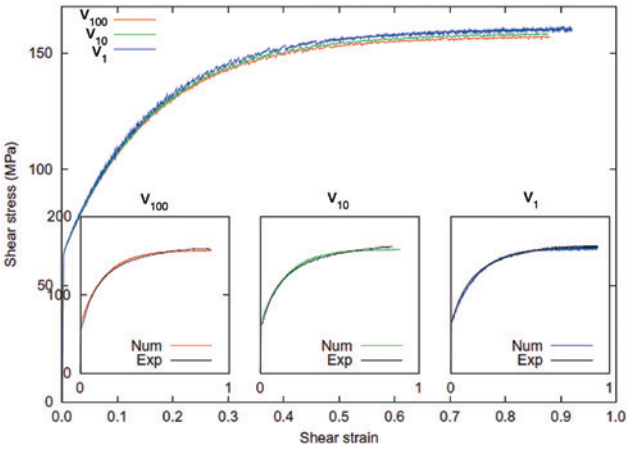

Figure 7: A comparison between the predicted and experimentally measured shear stress-shear strain curves.
These values are for an Al alloy using McCormick model for three different strain rates v_1, v_{10} and V_{100} representing $\dot{\gamma}$=1.2 e-3, $\dot{\gamma}$=1.2 e-2 and $\dot{\gamma}$=1.25 e-1 s^{-1}, respectively [49].

The parameters A, B, D, n, m and $\dot{\varepsilon}_0$ are material constants, and T is the non-dimensional temperature. The term $[A+B\bar{\varepsilon}^{P^n}]$ represents the plastic strain hardening (i.e. Ludwik's equation), $\left[1+D\ln\left(\frac{\dot{\bar{\varepsilon}}^P}{\dot{\varepsilon}_0}\right)\right]$ represents the strain rate hardening and the third term of $[1\text{-}T^m]$ indicates the thermal softening. In this relation, the PLC effect occurs when D is negative. For the simulation of the behaviour of these Al alloys, the Voce-type law was employed in Eq. (25). Hence, if the thermal effect is ignored, the following relation is used:

$$\bar{\sigma}=[\sigma_y+Q(1\text{-}\exp(\text{-}b\bar{\varepsilon}^P))]\left[1+D\ln\left(\frac{\dot{\bar{\varepsilon}}^P}{\dot{\varepsilon}_0}\right)\right]. \tag{26}$$

Generally, the work of Manach et al. [49] indicates that the McCormick model is capable of reproducing DSA in shear test at room temperature, and that the kinematics and morphology of the localised plastic bands are in a satisfying agreement with experimental results.

The Bergstrom and Hallen model is a physically-motivated material model based on dislocation densities [53]. The model has been used in thermomechanical coupled processes of warm forming of Al by Van den Boogaard and Huetink [54] and Palumbo et al. [55]. The model decomposes the flow stress in to three components: a strain and strain rate independent stress σ_0, a dynamic stress that depends on strain rate and temperature and a work hardening component. The flow stress was decomposed into a strain and strain rate independent stress σ_0 and σ_w, which incorporate work hardening as shown in the following relation:

$$\sigma_f=\sigma_0(T)+\sigma_w(\rho, T). \tag{27}$$

The work hardening-dependent stress, σ_w, is a function of the dislocation density ρ given by:

$$\sigma_w=\alpha G(T)b\sqrt{\rho}. \tag{28}$$

Here, G and b are the shear modulus and the Burgers vector, respectively, and α is a scaling parameter. The evolution of dislocation density is expressed as the competition between dislocation storage and recovery by remobilisation and annihilation expressed as:

$$\frac{d\rho}{d\varepsilon}=U(\rho)\text{-}\Omega(\dot{\varepsilon}, T)\rho, \tag{29}$$

where U represents the storage of mobile dislocations, and Ω is the dynamic recovery by remobilisation and annihilation. The amounts of Ω and U determine the shape of the hardening curve, which can be written as:

$$\Omega(\dot{\varepsilon}, T)=\Omega_0+C\exp\left(\frac{\text{-}mQ_V}{RT}\right)\dot{\varepsilon}^{\text{-}m}, \tag{30}$$

$$u(\rho)=U_0\sqrt{\rho}. \tag{31}$$

Palumbo et al. [55] also used the Bergstrom constitutive model to simulate warm deep drawing of AA-5xxx using coupled thermomechanical FE analysis. Deep drawing experiments were performed with a cooled punch and heated dies. Axisymmetric simulations were performed with various coefficients of friction and punch speeds. The calculated punch force had reasonable agreement with the experiments.

Kurukuri et al. developed an improved physically-based constitutive model known as the NES model [56]. The NES model improves on the Bergstrom model by incorporating a multiparameter description of microstructure. The dislocations are assumed to be stored in finite cells, and both the dislocation density and cell size are tracked. The cells are bounded by finite walls, and at large strains, the walls collapse due to dynamic recovery. The NES model has improved strain rate dependence over the Bergstrom model and can more accurately predict localisation. Kuruki recommended investigating friction in detail to improve warm forming simulations. The NES model requires 30 independent parameters to be fully defined.

3 Thermodynamic constitutive formulation

In the works of Rizzi and Hahner [57, 58] a model based on a thermodynamical approach was proposed. The model equations were developed in a one-dimensional context and processes were taken as isothermal. At the starting point, Rizzi's model assumes that plastic flow is brought by thermally-activated dislocation glide, similar to the other PLC models (e.g. McCormick's model). Hence, according to the constitutive flow rule of the Arrhenius type relation, the strain rate is given as:

$$\dot{\varepsilon}_t=\vartheta\Omega\exp\left(\text{-}\frac{G_0+\Delta G}{kT}+\frac{\sigma_{\text{ext}}\text{-}\sigma_{\text{int}}}{S_0}\right), \tag{32}$$

where ϑ and Ω are physical parameters representing the attempt frequency of thermal activation and the elementary plastic strain corresponding to the activation of all mobile dislocation segments, respectively. In addition, k represents Boltzmann constant and T is temperature.

The salient feature of the present PLC model is that the Gibbs free activation enthalpy G defining this energy barrier is considered a dynamic internal variable, which is subjected to the dynamic strain ageing. It can be written as:

$$G=G_0+\Delta G, \tag{33}$$

where G_0 is the basic activation enthalpy in the absence of DSA, and ΔG is an additional contribution related to DSA, which is in proportion to the solute concentration accumulated at the glide dislocation segments. In Eq. (32), the equivalent stress (σ_{eff}) does not coincide with the externally applied stress, σ_{ext}, given that only the excess of external stress over the internal stress σ_{int} resulting from dislocations as defects, is effective in driving dislocation motion. Both σ_{eff} and σ_{ext} are dynamic quantities that depend on DSA (due to ΔG), on plastic strain and on plastic strain rate. However, σ_{int} depends only on strain hardening given by:

$$\sigma_{\text{eff}}(\varepsilon, \dot{\varepsilon}_t, \Delta G)=\sigma_{\text{ext}}(\varepsilon, \dot{\varepsilon}_t, \Delta G)-\sigma_{\text{int}}(\varepsilon). \tag{34}$$

The material parameter S_0 in Eq. (32) defines the instantaneous strain rate sensitivity (SRS) of the flow stress with respect to processes that can be obtained by inverting the Arrhenius law [Eq. (32)]:

$$\sigma_{\text{ext}}(\varepsilon, \dot{\varepsilon}_t, \Delta G)=\sigma_{\text{int}}(\varepsilon)+S_0\frac{G_0}{kT}+S_0\ln\left(\frac{\dot{\varepsilon}_t}{\vartheta\Omega}\right)+S_0\frac{\Delta G}{kT}, \tag{35}$$

in which

$$S_0=\left.\frac{\partial\sigma_{\text{ext}}}{\partial\ln\dot{\varepsilon}_t}\right|_{\varepsilon,\,\Delta G}. \tag{36}$$

The instantaneous SRS, which relates as $S_0=kT/V$ to the activation volume V of the thermally-activated dislocation glide, is positive, that is, the flow stress always increases, almost instantaneously, with a sudden increase in strain rate. This does not imply, however, that the SRS actually governing the stability of plastic flow does not become negative. In fact, a change in strain rate is followed by a stress transient towards a new steady state, which may be above or below the extrapolated stress-strain curve before the strain-rate jump. This is accounted for by introducing the so-called asymptotic SRS S_∞, which assumes negative values in the PLC range. Formally, S_∞ is defined as the SRS of the flow stress as observed when DSA processes have relaxed to a new steady state expressed as

$$S_\infty=\left.\frac{\partial\sigma_{\text{ext}}}{\partial\ln\dot{\varepsilon}_t}\right|_{\varepsilon}=S_0+\left.\frac{\partial\sigma_{\text{ext}}}{\partial\Delta G}\right|_{\varepsilon}\frac{\mathrm{d}\Delta G}{\mathrm{d}\ln\dot{\varepsilon}_t}=S_0\left(1+\frac{1}{kT}\frac{\mathrm{d}\Delta G}{\mathrm{d}\ln\dot{\varepsilon}_t}\right). \tag{37}$$

According to Eq. (32), it can be pointed out that a constitutive equation of that type should be applied to each single active dislocation slip system. Accordingly, σ can be considered as the shear stresses resolved on the respective slip systems and the same for strains, i.e. $\dot{t}$ as the corresponding plastic shear strain rates $\dot{\gamma}_t$. In order to simplify this process, the resolved stresses and strains are rather replaced by the equivalent quantities. Another relevant point is that yielding, as represented here, is smooth without any discontinuous elastic to plastic transition ruled by a yield function. However, in reality, yielding turns out to be quite sharp, with a well-defined yield point due to the exponential term. Furthermore, aiming only at simulating tests with continuous plastic flow, material branching between plastic and unloading elastic responses is not taken into account. Notice that this does not impede local unloading associated to the plastic instabilities in the PLC range.

Rizzi and Hahner took an additional activation enthalpy G related to the kinetics of DSA as the main feature of his model. This is a (dynamic) internal variable of the model. The term ΔG is calculated as:

$$(\Delta G)_t=\eta(\Delta G_\infty-\Delta G)-\frac{\dot{\varepsilon}_t}{\Omega}\Delta G. \tag{38}$$

Through plastic deformation, when ageing occurs and dislocations are arrested at dislocation tangles, solute atoms diffuse towards the dislocations. Hence, the concentration of solute atoms on the dislocations increases, thus leading to an increase of the activation enthalpy ΔG. Afterwards, when dislocations are released by thermal activation, these escape from their solute clouds. Thus, the solute concentration, and hence the additional activation enthalpy, is reset to zero at a rate controlled by the plastic strain rate. DSA and then the PLC feature can be explained by the interplay of these two mechanisms.

In Eq. (38), when $\dot{\varepsilon}_t=0$ (during static ageing), $\Delta G=\Delta G_\infty(1-\exp(-\eta t))$ where the parameter η presents the ageing rate. For $t>>\eta^{-1}$ the additional activation enthalpy approaches the maximum value ΔG_∞ and for $t>>\eta^{-1}$ the solute concentration increases linearly resulting in $\Delta G\approx\Delta G_\infty\eta t^2$. The term of unpinning in Eq. (39) brings about the decrease of ΔG due to thermal activation, which occurs at a specific rate. The characteristic time scale of this process is the waiting time $t_w=\frac{\Omega}{\dot{\varepsilon}_t}$ spent by dislocations at the obstacles. This part of Eq. (38) is non-linear, which can be attributed to the dependence of $\dot{\varepsilon}_t$ on ΔG. The ratio of two time scales (i.e. η^{-1} and $\frac{\Omega}{\dot{\varepsilon}_t}$) governs the competition of the two processes and the resulting kinetics of DSA.

In a steady-state condition, where $\Delta G=0$ in Eq. (38), it can be written as follows:

$$\Delta G_s=\left(\frac{\Delta G_\infty}{1+\frac{\dot{\varepsilon}_t}{\Omega\eta}}\right). \tag{39}$$

Regarding Eq. (37) and $\frac{\mathrm{d}\Delta G}{\mathrm{d}\ln\dot{\varepsilon}_t}$ with $\Delta G=\Delta G_s$, the above relation becomes:

$$S_\infty=S_0\left(1-g_\infty\frac{\dot{\varepsilon}_t/\Omega\eta}{1+\dot{\varepsilon}_t/(\Omega\eta)^2}\right), \text{ where } g_\infty=kT. \tag{40}$$

Hence, SRS gets negative when:

$$\frac{g_\infty-2-\sqrt{g_\infty(g_\infty-4)}}{2}\equiv g_l<\frac{\dot{\varepsilon}_t}{\Omega\eta}<g_u\equiv\frac{g_\infty-2+\sqrt{g_\infty(g_\infty-4)}}{2}. \tag{41}$$

Here, SRS becomes zero at $g_\infty=4$ when the two characteristic time scales match each other (i.e. $\dot{\varepsilon}_t=\Omega\eta$). However, for the values of $g_\infty>4$, Eq. (10) defines the range of plastic strain rates that give rise to a negative SRS. In this relation, g_l and g_u are the lower and upper bounds, respectively, which are ruled by the saturation DSA enthalpy ΔG_∞. It is noticeable that the steady-state deformation condition is $\sigma_{\mathrm{ext},t}=h\dot{\varepsilon}_t$, so that Eq. (41) also provides the stress rates $g_l<\frac{\sigma_{\mathrm{ext},t}}{\Omega\eta h}<g_u$ entering the regime of a negative SRS.

With the goal of simplifying the equations, the non-dimensional driving force of f can be written as a function of σ_{eff}:

$$f\equiv f_0\exp\left(\frac{\sigma_{\mathrm{eff}}}{S_0}\right), \tag{42}$$

where the factor of f_0 $\left(f_0=\frac{\vartheta}{\eta}\exp\left(\frac{G_0}{kT}\right)\right)$ embeds the frequency of ϑ. Hence we have:

$$\dot{\varepsilon}_t=\eta\Omega\exp\left(-\frac{\Delta G}{kT}\right)f. \tag{43}$$

Taking the evolution equation of f by time differentiation, we have:

$$f_t=\left(\frac{\sigma_{\mathrm{ext},t}}{S_0}-\frac{h\dot{\varepsilon}_t}{S_0}\right)f. \tag{44}$$

Replacing relation (44) in Eqs. (45) and (39), the differential equations in f and ΔG become:

$$f_t=\frac{\sigma_{\mathrm{ext},t}}{S_0}f-\frac{h\eta\Omega}{S_0}\exp\left(-\frac{\Delta G}{kT}\right)f^2, \tag{45}$$

and

$$(\Delta G)_t=\eta(\Delta G_\infty-\Delta G)-\eta f\exp\left(-\frac{\Delta G}{kT}\right)\Delta G. \tag{46}$$

As seen in previous relations, the non-dimensional additional activation enthalpy variable as defined by the energy ratio $g=\frac{\Delta G}{kT}$ is employed. Considering $g_0=\frac{\Delta G_0}{kT}$, $g_s=\frac{\Delta G_s}{kT}$ and $g_\infty=\frac{\Delta G_\infty}{kT}$, the constitutive equations forming the base of the present model of the PLC effect are now expressed as:

$$\dot{f}=\dot{\sigma}f-\theta\exp(-g)f^2, \tag{47}$$

$$\dot{g}=g_\infty-g-f\exp(-g)g. \tag{48}$$

Here, the dimensionless stress rate $\dot{\sigma}$ and hardening coefficient θ are scaled parameters. These parameters are linked to $\sigma_{\mathrm{ext},t}$ and h using the relations below:

$$\dot{\sigma}=\frac{\sigma_{\mathrm{ext},t}}{\eta S_0} \text{ and} \tag{49}$$

$$\theta=\frac{h\Omega}{S_0}. \tag{50}$$

When the non-dimensional hardening coefficient of θ is smaller than 1 (i.e. weak hardening), f is the slow variable of the model, while g represents its fast variable in Eqs. (47) and (48).

In constitutive Eqs. (47) and (48), the incorporation of two available intrinsic time-scale parameters [one associated with ageing – unit time scale characteristic of g shown in Eq. (47) and the other one associated with strain hardening characteristic time θ governing f, Eq. (48)] constitutes a major difference between Rizzi's model and Penning's type models. The ratio between η^{-1} and $t_w=\frac{\Omega}{\dot{\varepsilon}_t}$ governs the appearance of the PLC effect, while θ determines the shape of the limit cycle in the weak hardening regime. Setting $\dot{g}=0$ in the Rizzi model may lead to the recovery of the other previous model: one recovers the flow stress rule Eq. (35), with ΔG replaced by its steady-state value ΔG_s, Eq. (39). Given that the strain-rate dependence of this flow stress is "N-shaped" (provided that $\Delta G_\infty>4kT$), this is formally equivalent to Penning's model (Figure 4).

This model was used in the work of Hahner et al. [59] to study the PLC band properties in a Cu-Al alloy. The simulated results were compared with those obtained by experiments in Figure 8. Here, in both simulated and experimentally measured curves, different types of

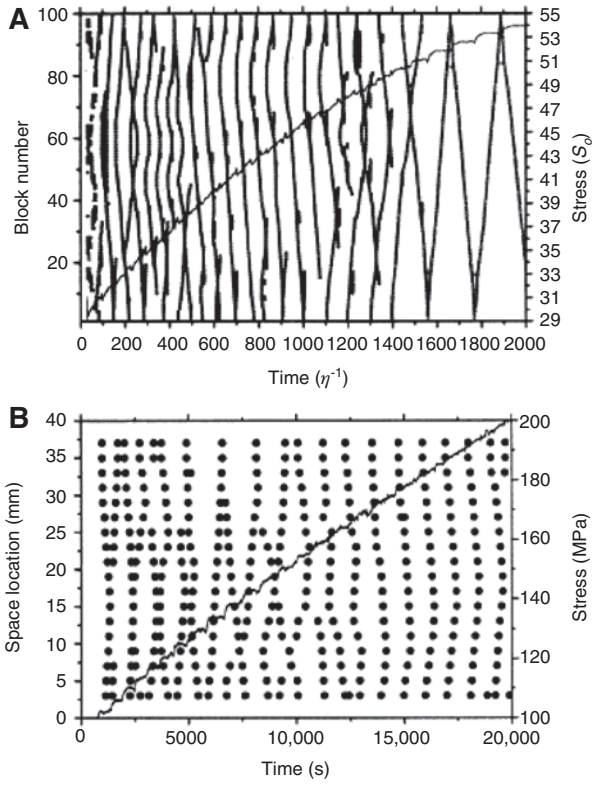

Figure 8: The PLC band properties in a Cu-Al alloy. (A) Space-time plot of band propagation for $\dot{\varepsilon}_2$=2E-6 s^{-1} obtained from the model. (B) Experimental space-time plot of band propagation [59].

propagating modes (e.g. multiple band propagation with band collisions, serration propagation with reflections at one end and parallel propagation) can be indicated. This study shows that the model is able to monitor the prominent features of PLC bands in this material. The details of the numerical results are in good agreement with the analytic expressions for the band velocity, strain and width.

4 Conclusion

In this research, various constitutive approaches to explain the serration behaviour in metallic alloys induced by the PLC effect have been studied. The theoretical interpretation and modelling of this plastic instability in materials was first suggested by the Penning and then developed later on by McCormick, Ling, Estrin, and Kubin during last decades. The previous works indicated that the model of McCormick, as a micromechanical constitutive formulation, has potential to describe the PLC effects in different materials in terms of different types of PLC effects and statistical observation. The simulated results are in good agreement with the experimental observations. Concerning 3D simulations, however, the model of Zhang, which had originally been reformulated from the McCormick model, indicates accurate descriptions of PLC effect in engineering samples. Furthermore, the models of Rizzi and Hahner are also used to study the serration behaviour of the materials considered in this review. This model, which is based on thermodynamic relations, has been evaluated in this work. The significant aspect of this approach is the consideration of the Gibbs free activation enthalpy as the energy barrier subject to dynamic strain ageing. Investigations on the PLC effect using this idea indicate that the Rizzi and Hahner models are able to predict the PLC band propagation in the material.

Acknowledgments: This work was co-financed by the Portuguese Foundation for Science and Technology via project PTDC/EMS-TEC/1805/2012 and by FEDER via the 'Programa Operacional Factores de Competitividade' of QREN.

References

[1] Winstone MR, Rawlings RD, West DRF. *J. Less Comm. Metals.* 1973, 31, 143–150.
[2] Mulford RA, Kocks UF. *ACTA Metall.* 1979, 27, 1125–1134.
[3] Van den Beukel A, Kocks UF. *ACTA Metall.* 1982, 30, 1027–1034.
[4] Schwarz RB. *Scripta Metall.* 1982, 16, 385–390.
[5] Piobert A. *Mem. Artillerie.* 1842, 5, 525.
[6] Lüders W. *Dinglers Polytech. J.* 1860, 155, 18.
[7] Subramanian KH, Duncan AJ. *Tensile Properties for Application to Type I and Type II Waste Tank Flaw Stability Analysis (U), WSRC-TR-2000-00232*, Westinghouse Savannah River Company, Aiken: SC, 2000.
[8] Savart F. Recherches sur les vibrations longitudinales Annales de Chimie et de Phisique, 2nd series, 1837, 65.
[9] Le Chatelier F. *Rev. Métall.* 1909, 6, 914–917.
[10] Portevin A, Le Chatelier F. *Comptes Rendus de l'Académie des Sciences Paris.* 1923, 176, 507–510.
[11] Nabarro FR, Theory of crystal dislocations. Oxford: Clarendon Press, 1967.
[12] Brindley BJ, Worthington PJ. *Metall. Rev.* 1970, 15, 101–114.
[13] Robinson JM. *Int. Mater. Rev.* 1994, 39, 217–227.
[14] Gremaud G. *Mater. Sci. Eng. A.* 2004, 370, 191–198.
[15] Picu RC. *ACTA Mater.* 2004, 52, 3447–3458.
[16] Serajzadeh S, Sheikh H. *Mater. Sci. Eng. A.* 2008, 486, 138–145.
[17] Chinh QN, Horvath G, Kovacs Z, Juhasz A, Berces G, Lendvai J, *Mater. Sci. & Eng. A* 2005, 409, 100–107.
[18] Penning P. *ACTA Metall.* 1972, 20, 1169–1175.
[19] Kubin LP, Estrin Y. *ACTA Metall.* 1985, 33, 397–407.
[20] Chihab K, Estrin Y, Kubin LP, Vergnol J. *Scripta Metall.* 1987, 21, 203–208.
[21] McCormick PG. *ACTA Metall.* 1988, 36, 3061–3067.

[22] McCormick PG. *Proc. ICSMA.* 1988, 8, 409–414.
[23] Estrin Y, McCormick PG. *ACTA Metall. Mater.* 1991, 39, 2977–2983.
[24] McCormick PG, Estrin Y, Lowe TC, Rollett AD, Follansbee PS, Daehn GS. *Modelling the Deformation of Crystalline Solids*, TMS: Warrendale, 1991, p 293.
[25] McCormick PG, Ling CP. *ACTA Metall. et Mater.* 1995, 43, 1969–1977.
[26] Kubin LP, Chihab K, Estrin Y. ACTA Metall. 1988, 36, 2707–2718.
[27] Kubin LP, Estrin Y. *ACTA Metall. et Mater.* 1990, 38, 697–708.
[28] Louat N. *Scripta Metall.* 1981, 15, 1167–1170.
[29] Estrin Y, Kubin LP. *J. Mech. Behavior Mater.* 1989, 2, 255–292.
[30] Cottrell AH, Bilby BA. *Proc. Phys. Soc. A* 1949, 62, 49.
[31] Kalk A, Schwink CH. *Phys Status Solidi B* 1992, 172, 133–144.
[32] Ling CP, McCormick PG. *ACTA Metall. et Mater.* 1990, 38, 2631–2635.
[33] Ling CP, McCormick PG. *ACTA Metall. et Mater.* 1993, 41, 3127–3131.
[34] Jiang H, Zhang Q, Chen X, Chen Z, Jiang Z, Wu X, Fan XJ. *ACTA Mater.* 2007, 55, 2219–2228.
[35] Lebyodkin M, Brechet Y, Estrin Y, Kubin L. *ACTA Mater.* 1996, 44, 4531–4541.
[36] Lebyodkin M, Dunin-Barkowskii L, Brechet Y, Estrin Y, Kubin LP. *ACTA Mater.* 2000, 48, 2529–2541.
[37] Zhang S, McCormick PG, Estrin Y. *ACTA Mater.* 2001, 49, 1087–1094.
[38] Estrin Y. Dislocation-density-related constitutive modelling. In *Unified Constitutive Laws of Plastic Deformation*, Krausz, AS, Krausz, K, Eds., Academic Press: New York, 1996, p. 69.
[39] Kok S, Beaudoin AJ, Tortorelli DA, Lebyodkin M. *Mod. Sim. Mater. Sci. Eng.* 2002, 10, 745.
[40] Kok S, Beaudoin AJ, Tortorelli DA, Lebyodkin M, Kubin L, Fressengeas C. *J. Phys. IV* 2003, 105, 191–197.
[41] Graff S, Forest S, Strudel JL, Prioul C, Pilvin P, Bechade JL. *Mater. Sci. Eng. A.* 2004, 387, 181–185.
[42] Graff S, Forest S, Strudel JL, Prioul C, Pilvin P, Bechade JL. *Scripta Mater.* 2005, 52, 1181–1186.
[43] Belotteau J, Berdin C, Forest S, Parrot A, Prioul C. *Mater. Sci. Eng. A* 2009, 526, 156–165.
[44] Maziere M, Besson J, Forest S, Tanguy B, Chalons H, Vogel F. *Euro. J. Mech. A/Solids* 2009, 28, 36–44.
[45] Hopperstad OS, Borvik T, Berstad T, Lademo OG, Benallal A. *Mod. Sim. Mater. Sci. Eng.* 2007, 15, 747–772.
[46] Wenman MR, Chard-Tuckey PR. *Int. J. Plasticity* 2010, 26, 1013–1028.
[47] Benallal A, Berstad T, Borvik T, Clausen AH, Hopperstad OS. *Eur. J. Mech. A-Solid* 2006, 25, 397–424.
[48] Clausen AH, Borvik T, Hopperstad OS, Benallal A. *Mater. Sci. Eng. A* 2004, 364, 260–272.
[49] Manach PY, Thuillier S, Yoon JW, Coer J, Laurenta H. *J. Plasticity* 2014, 58, 66–83.
[50] Wang HD, Berdin C, Maziere M, Forest S, Prioul C, Parrot A, Le-Delliou P. *Mater. Sci. Eng. A* 2012, 547, 19–31.
[51] Johnson GR, Cook WH. *Pro. 7th Int. Symp. Ballistics* 1983, 21, 541–547.
[52] Johnson GR, Cook WH. *Eng. Fract. Mech.* 1985, 21, 31–48.
[53] Bergstrom Y, Hallen H. *Mater. Sci. Eng.* 1982, 55, 49–61.
[54] Van den Boogaard AH, Huetink J. *Comput. Methods Appl. Mech. Eng.* 2006, 195, 6691–6709.
[55] Palumbo G, Sorgente D, Tricarico L, Zhang SH, Zheng WT. *J. Mater. Pro. Tech.* 2007, 191, 342–346.
[56] Kurukuri S, Van den Boogaard AH, Miroux A, Holmedal B. *J. Mater. Pro. Tech.* 2009, 209, 5636–5645.
[57] Hahner P, Rizzi E. *ACTA Mater.* 2003, 51, 3385–3397.
[58] Rizzi E, Hahner P. *J. Plasticity* 2004, 20, 121–165.
[59] Hahner P, Ziegenbein A, Rizzi E, Neuhausser H. *Phy. Rev. B* 2002, 65, 134109.